



# Comparison of supercontinuum generation spectral intensity in benzene-core PCFs with different types of lattices in the claddings

L. Chu Van<sup>1</sup> · B. T. Le Tran<sup>1</sup> · T. Nguyen Thi<sup>2</sup> · D. Hoang Trong<sup>2</sup> · T. Dang Van<sup>1</sup> · T. Do Mai<sup>1</sup> · H. Trinh Ngoc<sup>1</sup> · T. Thai Doan<sup>3</sup> · K. Doan Quoc<sup>4</sup>

Received: 1 April 2022 / Accepted: 16 September 2022

© The Author(s), under exclusive licence to Springer Science+Business Media, LLC, part of Springer Nature 2022

## Abstract

Three newly designed benzene-core photonic crystal fibers (BC-PCFs) can optimize both chromatic dispersion and attenuation characteristics simultaneously for the most efficient application to generate supercontinuum. The nonlinear characteristics of BC-PCFs with the circular lattice (CL), square lattice (SL), and hexagonal lattice (HL) are analyzed numerically to select the optimal PCF. The three optimized structures: #CBF<sub>1</sub>, #SBF<sub>2</sub>, and #HBF<sub>3</sub> are intended for supercontinuum generation (SCG) in an all-normal dispersion regime. The obtained results demonstrated that although #HBF<sub>3</sub> fiber has a larger effective mode area and attenuation than #CBF<sub>1</sub>, #SBF<sub>2</sub> fibers, the dispersion curve of #HBF<sub>3</sub> is flattest and closest to the zero-dispersion curve in the wavelength region of 0.8–2.0 μm hence it has the highest efficiency for SCG. These PCFs are capable of coherent octave-wide SCG in the 0.66–1.53 μm, 0.71–1.76 μm, and 0.71–1.82 μm wavelength ranges with low peak power of 0.45 kW and 40 fs pulses coupled to the core. Those fibers are the real objects for the sources of all-fiber supercontinuum, which can be substituted for glass core fibers because the nonlinearity of silica is lower than that of benzene. The proposed remedy can lead to new low-cost all-fiber optical systems.

**Keywords** Benzene · Circular lattice · Hexagonal lattice · Square lattice · Coherent octave-wide SCG

---

✉ L. Chu Van  
chuvanlanh@vinhuni.edu.vn

✉ K. Doan Quoc  
doanquockhoa@tdmu.edu.vn

<sup>1</sup> Vinh University, 182 Le Duan, Vinh, Vietnam

<sup>2</sup> University of Education, Hue University, 34 Le Loi Street, Hue, Vietnam

<sup>3</sup> Ho Chi Minh City University of Food Industry, 140 Le Trong Tan, Tan Phu, Ho Chi Minh City, Vietnam

<sup>4</sup> Institute of Applied Technology, Thu Dau Mot University, Binh Duong Province, Vietnam

## 1 Introduction

SCG is an extensively researched phenomenon that can appear in an optical medium due to the associated effects of the medium's dispersion and nonlinearity (Dudley et al. 2006). Supercontinuum light depicts an original and flexible source of ultra-broadband radiation with the high-power density of the spectra and a high degree of coherence tantamount to a white-light laser. Thanks to this outstanding feature, SCG has created enormous applications in science and technology such as in spectroscopy (Ulman et al. 1993; Kano and Hamaguchi 2005; Isobe et al. 2009), optical coherence tomography (Hartl et al. 2001), pulse compression (Heidt et al. 2011; Tu et al. 2011; Hooper et al. 2011), tunable lasers (Takushima and Kikuchi 1999), and optical frequency metrology (Udem et al. 2002).

PCF discovery has significantly innovated SCG technology. One reason for this is the versatility of dispersion techniques, which allows it to shift the zero-dispersion wavelength (ZDW) to briefer wavelengths (Mogilevtsev et al. 1998). This allows obtaining the broadest spectrum by pumping in the anomalous dispersion system. An additional advantage of PCF is its ability to restrict light tightly to its core, increasing nonlinearity and thus SCG efficiency, i.e., for bandwidth enhancement (Ranka et al. 2000). Furthermore, different effects of the nonlinear characteristic can control the expansion depending on the input combination of pump energy, pulse duration, pump wavelength, fiber nonlinearity, and fiber length (Dudley and Taylor 2010).

The nonlinear dynamics of SCG strongly depend on two dispersion regimes. Consider the first case of SCG in the anomalous dispersion region. In this way, PCF has to contain ZDW and the wavelength of the pump selected needs to be larger but closer to ZDW. This mechanism can create a broad SC spectrum with low energy. Nevertheless, the limitation of this approach is the weak coherence spectrum and large noise, which are caused by soliton dynamics and are extremely sensitive to the fluctuations of the pump pulse (Corwin et al. 2003; Qian et al. 2018). For the SCG in the all-normal dispersion regime of the fiber, although the spectral bandwidths are drastically reduced and the input energy is higher, the soliton effect can eliminate. In this situation, the spectral widening appears only via SPM and OWB so it is not only insensitive to the fluctuations of the pump pulse but also creates a high coherent SCG with low noise (Dudley and Taylor 2010; Heidt et al. 2017).

In addition, the efficiency of SCG depends on three important characteristics of PCF: dispersion, effective mode area, and attenuation (Dudley et al. 2006). These features can be controlled by changing the lattice shape in the cladding, the air hole dimensions, the lattice constant, and the solid or hollow core since PCF is very flexible in design compared to conventional optical fibers (COFs) (Knight et al. 1996; Buczyński 2004). SCG is most effective when the obtained dispersion curve is flat and close to the zero-dispersion curve and at the same, the effective mode area and attenuation are as small as possible (Corwin et al. 2003).

Commonly, the created lattices in cladding include CL, HL, and SL. Some publications have mentioned these lattices PCF such as a new CL-PCF with a large mode area (Medjouri et al. 2015), CL-PCF with high negative dispersion and ultra-low confinement loss (Pandey et al. 2020), the investigation confinement loss in HL-PCFs (Monfared et al. 2013), HL-PCF based optical sensor with a rotated-hexacore region (Sen et al. 2020), supercontinuum source for dense wavelength division multiplexing in SL-PCF (Saghaei 2017), and so forth. These publications analyzed structural parameters that influence the characteristics of PCFs for each lattice type, but they did not consider their applications in optics fiber technology. Additionally, these publications have

not proven which lattice of PCF is most efficient for SCG. The most recent publication (Tran et al. 2020) has analyzed the characteristic quantities of solid-core PCFs with various lattice types, but the authors have not yet applied the obtained results to generate SC due to the small nonlinear refractive index of the silica solid core. If this PCF applies to SCG, the obtained efficiency cannot be high. It is worth noting that the air hole diameters of lattice rings in the photonic cladding of these structures are the same. Therefore, they cannot optimize the chromatic dispersion and attenuation characteristics of PCF simultaneously. The cross-section of the mentioned fibers is introduced in Fig. 1.

In this paper, we use a commercial numerical model solution (LMS) software (<https://www.lumerical.com/products/mode/>) to design three new hollow-core PCF structures infiltrated with benzene including CL, HL, and SL. We emphasize the selection of benzene to fill the hollow core PCF because of its high nonlinear refractive index, with  $n_2 = 168 \times 10^{-20} \text{ m}^2 \text{ W}^{-1}$  at  $1.064 \mu\text{m}$ . Besides, another advantage of benzene is low attenuation in the broadband range of  $0.5\text{--}14 \mu\text{m}$  without high absorption peaks in this area (Nibbering et al. 1995). The rest of this study is organized as follows. In Sect. 2, we describe the schematic of the geometrical structure of PCFs with different types of lattice. The structural parameter's influence on the dispersion characteristics is analyzed to find the optimal structures with all-normal dispersion. Subsequently, we compare the characteristic quantities of these optimal structures as well as the spectral intensity

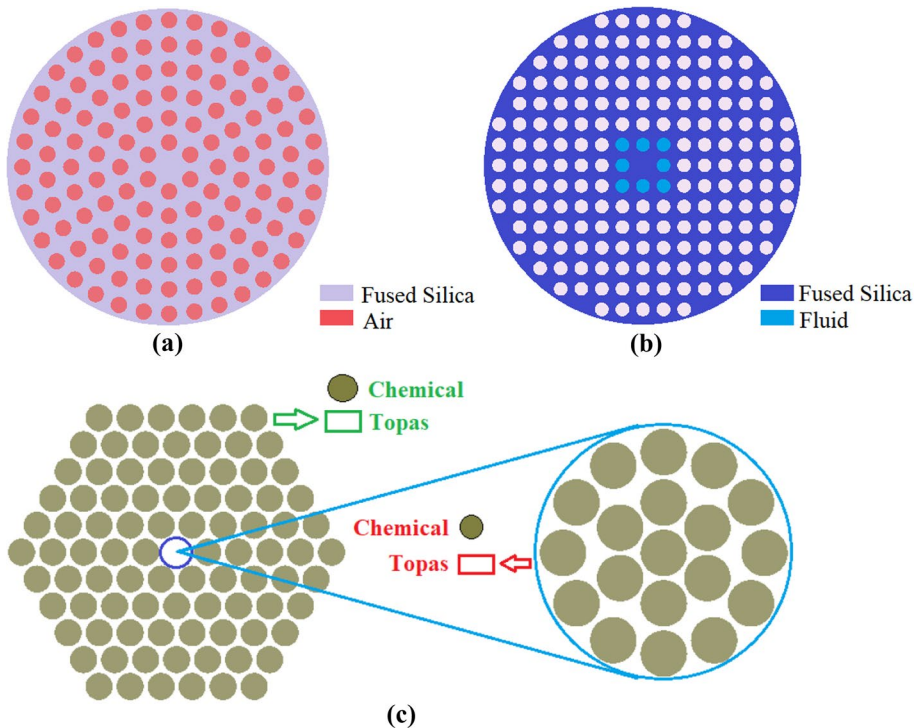


**Fig. 1** The cross-section of PCFs in publications **a** (Medjouri et al. 2015), **b** (Saghaei 2017), and **c** (Sen et al. 2020)

expansion in the SCG to show the PCF with the highest SCG efficiency in Sect. 3. The paper is closed with the conclusion in Sect. 4.

## 2 Numerical modeling of properties of PCFs

By using the finite-difference eigenmode (FDE) method with a commercial LMS(<https://www.lumerical.com/products/mode/>), the geometrical structure of benzene-core PCFs (BC-PCFs) with different lattices is modeled as shown in Fig. 2. In the FDE method, the cross-section of the fiber is divided into many rectangular sections. Each section has a size of 0.08  $\mu\text{m}$ . The boundary condition for the simulation herein is perfectly matched layer (PML) boundaries. This boundary condition allows the radiation to propagate out of the computational area without either an interferometer with the field inside or boundaries absorbing incident light upon them. The common features shared among the three structures (a), (b), and (c) are that the base material is fused silica glass and benzene is filled with a hollow core, and that the cladding includes eight rings of air-holes with diameter  $d$ . The lattice constant  $\Lambda$  and the cladding factor of linear filling are defined as  $f = d/\Lambda$ . The publication (Saitoh et al. 2003) has shown that the first ring size of air holes has the top influence on the dispersion properties, while the remaining rings affect the attenuation of PCF. Thus, we introduce a new design with the following structural parameters:

- The filling factor of the first ring ( $f_1 = d_1/\Lambda$ ) is changed from 0.3 to 0.8 in steps of 0.05.
- The other rounds have a constant filling factor  $f_2 = d_2/\Lambda$  of 0.95.
- The core diameter  $D_c$  is determined by the formula:  $D_c = 2\Lambda - 1.1d_1$ .
- The constants of the lattice  $\Lambda$ : 1.0, 1.5, 2.0, and 2.5  $\mu\text{m}$ .

where  $d_1$  and  $d_2$  are the diameters of the first and remaining ring air holes, respectively. This model allows the created PCFs to obtain minimum attenuation, and the ability to control the structural parameters to achieve optimal dispersion. This is probably the most significant feature of our design. It is completely different from previous works (Zhang et al. 2010; Van et al. 2017, 2020; Hoang et al. 2018), which showed no difference in the filling factor of the first rings and subsequent rounds.

The BC-PCFs can be fabricated by conventional stack-and-draw methods (Pysz et al. 2014). Liquid infiltrates into the core based on a laser writing technique (Vieweg et al. 2010), or thermal fusion splicer (Hoang et al. 2018) through integration with a microfluidic pump system (Hoang et al. 2018). We experimentally measured material

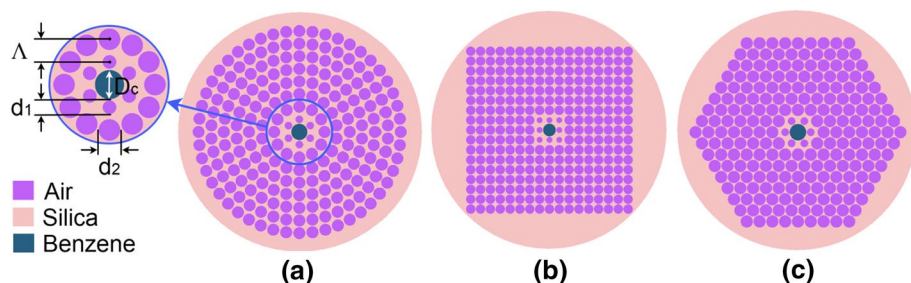


**Fig. 2** The geometrical structure of BC-PCFs with **a** CL, **b** SL, and **c** HL

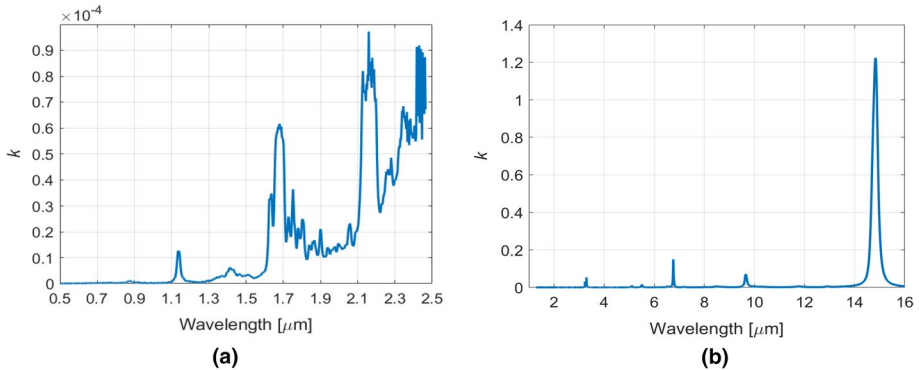
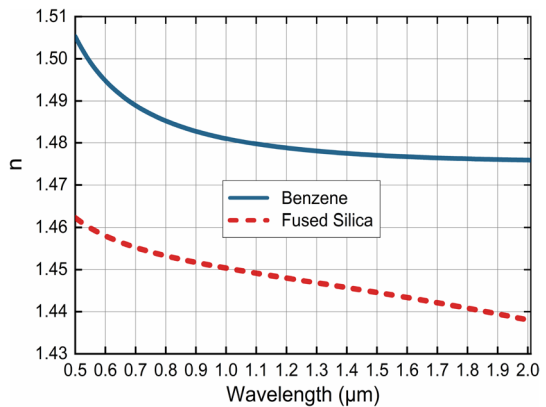


**Fig. 3** The imaginary part of the refractive index  $k$  of benzene, **a** measured and **b** after Ref (Myers et al. 2018)

**Fig. 4** Real parts of the refractive index of benzene and fused silica



attenuation of benzene for visible and near-IR wavelength ranges using a sample in a standard 10 mm cuvette. The illumination source was a halogen lamp, while the spectrum was analyzed using two spectrometers: Thorlabs CCS200 (range 0.2–1.0  $\mu\text{m}$ ) and Ocean NIR-QUEST (range 0.9–2.5  $\mu\text{m}$ ). The characteristic of the attenuation as the imaginary part of the linear refractive index  $k$  is shown in Fig. 3a. For the wavelength range, 1.28–16  $\mu\text{m}$  attenuation was adopted after Myers et al. (See Fig. 3b (Myers et al. 2018)) The core diameter of a PCF is a tradeoff between keeping it small to enable dispersion engineering through the photonic cladding design and keeping it large to match the mode field to standard telecom single-mode fibers as much as possible. In our case, benzene has a higher refractive index than silica (Fig. 4), so the fiber is an effective index-guiding PCF with the advantage of reasonably large mode field diameter and dispersion profile matched to important femtosecond lasers, such as erbium lasers centered at 1.56  $\mu\text{m}$ .

The real part of the linear refractive index  $n$  of benzene as a wavelength function is described using the Cauchy formula shown in Eq. 1 (Moutzouris et al. 2014), while the Sellmeier formula is applied for fused silica glass (SCHOTT Lithosil<sup>®</sup>) as shown in Eq. 2 (Tan 1998). The wavelength  $\lambda$  has dimensions of micrometers ( $\mu\text{m}$ ).

$$n_b(\lambda) = \sqrt{2.170184597 + 0.000593990\lambda^2 + \frac{0.023034640}{\lambda^2} + \frac{0.000499485}{\lambda^4} + \frac{0.000178796}{\lambda^6}}, \tag{1}$$

$$n_s(\lambda) = \sqrt{1 + \frac{0.6694226\lambda^2}{\lambda^2 - 4.4801 \times 10^{-3}} + \frac{0.4345839\lambda^2}{\lambda^2 - 1.3285 \times 10^{-2}} + \frac{0.8716947\lambda^2}{\lambda^2 - 95.341482}}. \tag{2}$$

The chromatic dispersion  $D$  is one of the significant factors for the SCG. It consists of the waveguide and material dispersion and is determined as given in Eq. 3 (Buczyński 2004):

$$D = -\frac{\lambda}{c} \frac{d^2(\text{Re}[n_{eff}])}{d\lambda^2}, \tag{3}$$

where  $\text{Re}[n_{eff}]$  depicts the real part of the effective refractive index of a guided mode.

Figures 5, 6, 7, and 8 present the dispersion characteristics of BC-PCFs with different values of lattice constant and the filling factor. From the graph, it can be seen that while the small core fibers ( $\Lambda = 1 \mu\text{m}$ ) have significant shifts in the dispersion by varying  $\Lambda$  and  $d_f/\Lambda$ , the dispersion shift of the larger ones is moderate. For CLs and SLs, the dispersion with two ZDWs exists when  $f_1 \geq 0.7$ , and all-normal dispersions achieve when  $f_1 = 0.45\text{--}0.65$ . (Fig. 5a, b). Figure 5c shows that, with  $f_1 \geq 0.55$ , the HLs have two ZDWs, but we get all-normal dispersions only for  $f_1$  close to 0.5. Due to the negative

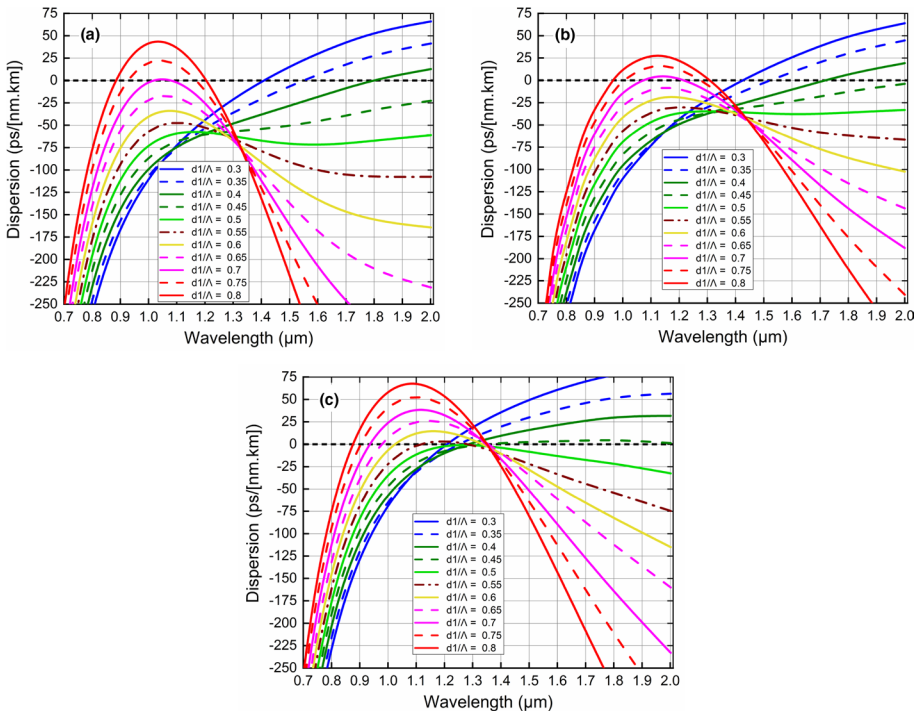


**Fig. 5** Dispersion characteristics of the fundamental mode for BC-PCFs:  $\Lambda = 1 \mu\text{m}$ ,  $f_1 = 0.3\text{--}0.8$  with **a** CL, **b** SL, and **c** HL



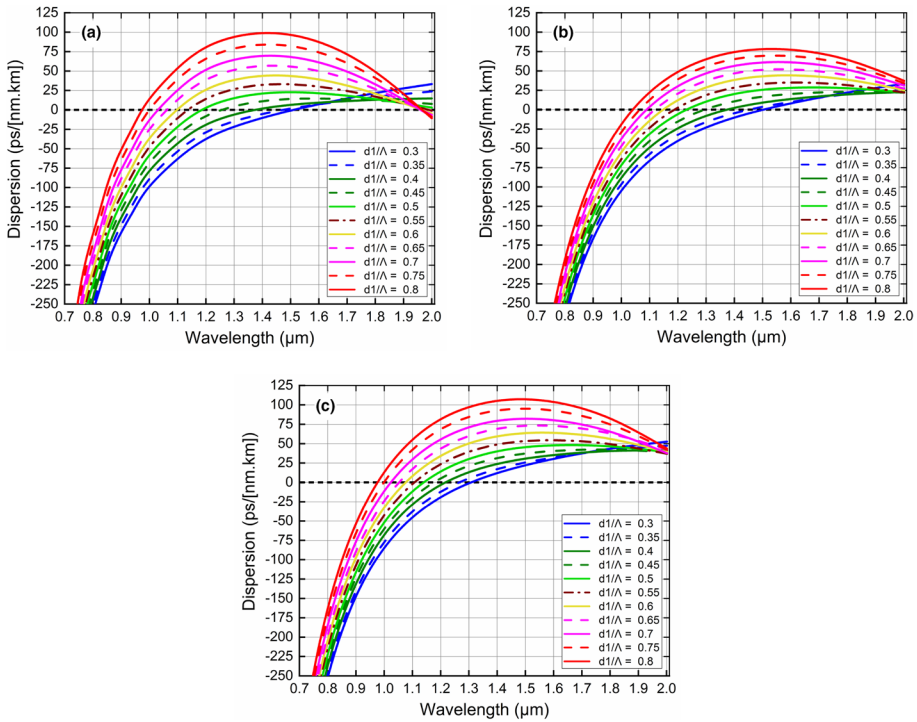


**Fig. 6** Dispersion characteristics of the fundamental mode for BC-PCFS:  $\Lambda = 1.5 \mu\text{m}$ ,  $f_1 = 0.3\text{--}0.8$  with **a** CL, **b** SL, and **c** HL

effects of the material dispersion of  $\text{C}_6\text{H}_6$ , the large core fibers have anomalous dispersion in the range  $\lambda > 1 \mu\text{m}$  (Figs. 6, 7, 8).

Next, we optimize the dispersion characteristic by choosing fiber structures with flat, near-zero dispersion curves and pump wavelength compatible ZDWs allowing a broader SCG to obtain further. Based on the preliminary simulation, three fibers corresponding to CL, SL, and HL are selected to analyze the SCG. They are labeled as #CBF<sub>1</sub>, #SBF<sub>2</sub>, and #HBF<sub>3</sub>. The dispersion characteristics of the fundamental mode for the proposed PCFs are presented in Fig. 9a. All fibers are used for SCG in an all-normal dispersion regime. The first structure, #CBF<sub>1</sub>, with  $\Lambda = 1.0 \mu\text{m}$ ,  $f_1 = 0.65$ , and  $D_c = 1.285 \mu\text{m}$ , is pumped at  $1.064 \mu\text{m}$ . The dispersion equals  $-17 \text{ ps}\cdot\text{nm}^{-1}\cdot\text{km}^{-1}$  at the pumped wavelength. The second fiber, #SBF<sub>2</sub> ( $\Lambda = 1.0 \mu\text{m}$ ,  $f_1 = 0.65$ , and  $D_c = 1.285 \mu\text{m}$ ), is expected to pump at the wavelength  $1.3 \mu\text{m}$ , when its dispersion is  $-19.9 \text{ ps}\cdot\text{nm}^{-1}\cdot\text{km}^{-1}$ . The third fiber, #HBF<sub>3</sub>, with structural parameters  $\Lambda = 1.0 \mu\text{m}$ ,  $f_1 = 0.5$ , and  $D_c = 1.450 \mu\text{m}$  has the nearest dispersion to the zero-dispersion curve. It is used for the same pump wavelength as the second fiber, with the value of dispersion at  $-0.89 \text{ ps}\cdot\text{nm}^{-1}\cdot\text{km}^{-1}$ .

Figure 9b indicates the attenuation characteristics of the fundamental mode for #CBF<sub>1</sub>, #SBF<sub>2</sub>, and #HBF<sub>3</sub>. The attenuation of #CBF<sub>1</sub> at  $1.064 \mu\text{m}$  is equal to  $0.18 \text{ dB/cm}$  while the attenuation of #SBF<sub>2</sub> and #HBF<sub>3</sub> at  $1.3 \mu\text{m}$  are equal to  $0.38$  and  $0.41 \text{ dB/cm}$ , respectively. When the wavelength is  $1.66 \mu\text{m}$ , the loss reaches the biggest values which are  $11.2$ ,  $11.3$ , and  $12.8 \text{ dB/cm}$  for #CBF<sub>1</sub>, #SBF<sub>2</sub>, and #HBF<sub>3</sub>, respectively.

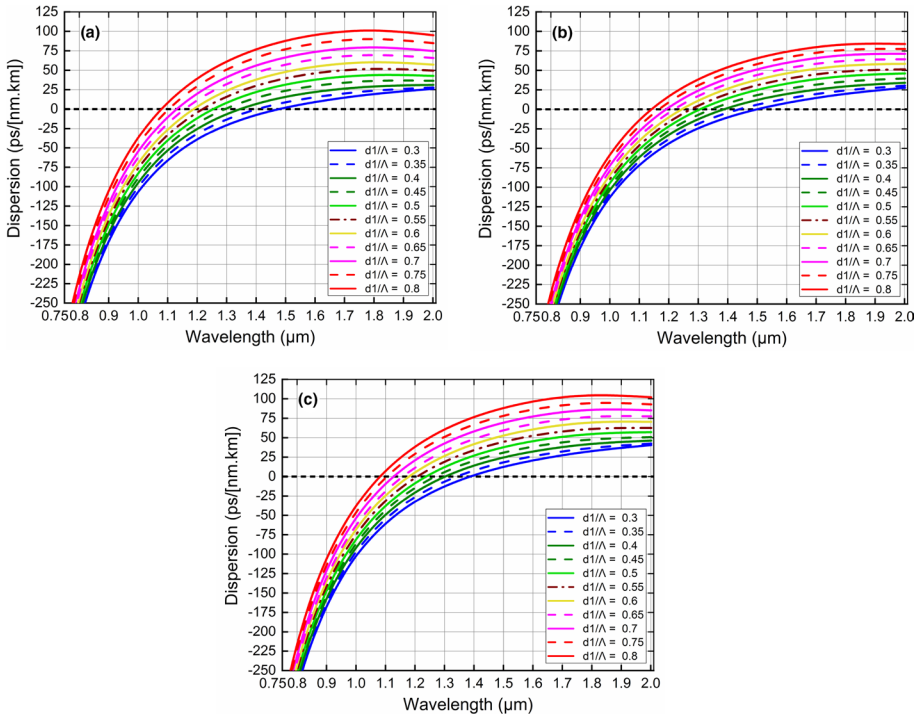


**Fig. 7** Characteristics of dispersion of the fundamental mode for BC-PCFS:  $\Lambda = 2.0 \mu\text{m}$ ,  $f_1 = 0.3\text{--}0.8$  with **a** CL, **b** SL, and **c** HL

The effective mode areas and nonlinear coefficients of the fundamental mode for #CBF<sub>1</sub>, #SBF<sub>2</sub>, and #HBF<sub>3</sub> fiber are shown in Fig. 10. Normally, the effective mode area has significantly dominated by the core diameter of the fiber, and thus its value is low for the small core fibers. Although #CBF<sub>1</sub> and #SBF<sub>2</sub> fibers have the same core diameter, #CBF<sub>1</sub> fiber has a lower effective mode area than #SBF<sub>2</sub> in the investigated wavelength region. This may be due to the difference in the lattice structure of the two PCFs. The effective mode area of #CBF<sub>1</sub> fiber at the wavelength of 1.064  $\mu\text{m}$  is equal to 1.33  $\mu\text{m}^2$  and these values are 1.84  $\mu\text{m}^2$ , 1.88  $\mu\text{m}^2$  at 1.3  $\mu\text{m}$  for #SBF<sub>2</sub>, and #HBF<sub>3</sub>, respectively.

The coefficient of the nonlinearity  $\gamma$  is calculated by the formula  $\gamma = 2\pi n_2 / \lambda A_{eff}$ , where  $A_{eff}$  is the area of the effective mode for the basic mode of the fiber (See Fig. 10b). With the high nonlinear refractive index of benzene, the proposed PCFs have large nonlinear coefficients. For  $\gamma$  is an inverse ratio of the effective mode area, fibers with the lowest effective mode area will have a higher nonlinear coefficient. The nonlinear coefficient of #CBF<sub>1</sub> at 1.064  $\mu\text{m}$  is equal to 7447  $\text{W}^{-1} \text{km}^{-1}$ , meanwhile #SBF<sub>2</sub>, and #HBF<sub>3</sub> have nonlinear coefficients of 5391, and 5255  $\text{W}^{-1} \text{km}^{-1}$  at 1.3  $\mu\text{m}$ , respectively. To emphasize the advantages of the proposed fibers, these fibers' properties are compared with those previously published. The data are presented in Table 1.



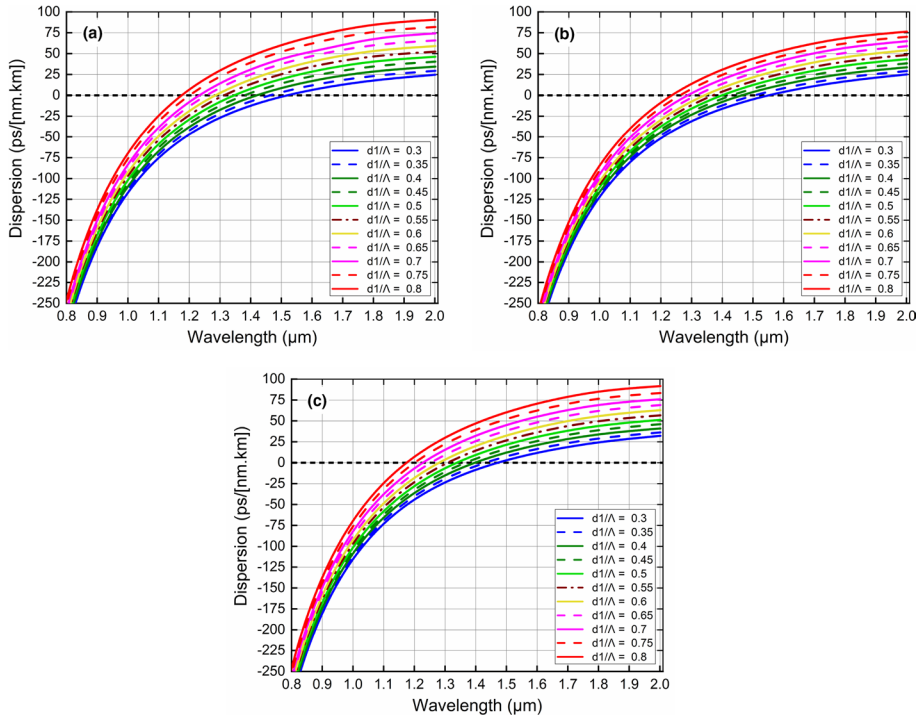


**Fig. 8** Characteristics of dispersion of the fundamental mode for BC-PCFS:  $\Lambda = 2.5 \mu\text{m}$ ,  $f_1 = 0.3\text{--}0.8$  with lattices **a** CL, **b** SL, and **c** HL

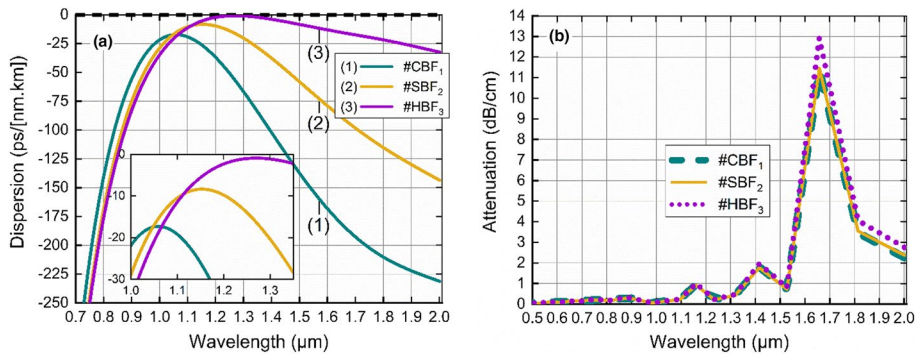


**Fig. 9** Characteristics of **a** dispersion and **b** attenuation of the fundamental mode for #CBF<sub>1</sub>, #SBF<sub>2</sub>, and #HBF<sub>3</sub>

### 3 SCG in the proposed fiber

SCG in the investigated fibers is numerically simulated by solving the equation of generalized nonlinear Schrödinger (GNLSE), using the symmetry split-step Fourier transform method (Dudley and Taylor 2010):

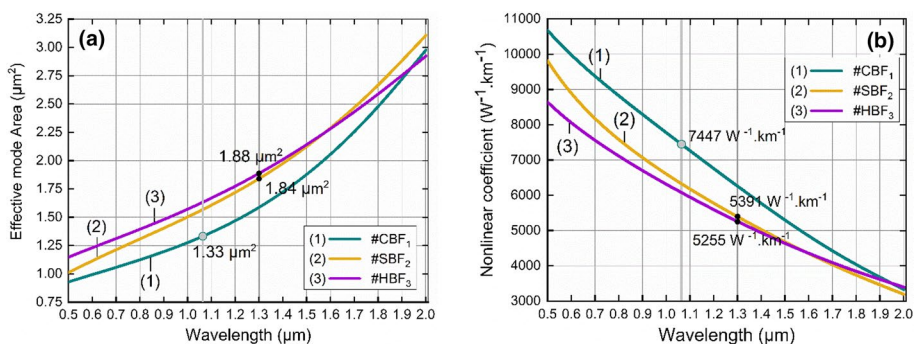


**Fig. 10** Characteristics of **a** effective mode area and **b** nonlinear coefficient of the fundamental mode for #CBF<sub>1</sub>, #SBF<sub>2</sub>, and #HBF<sub>3</sub>

**Table 1** The characteristic values of the proposed fibers are compared with those previously publications in the all-normal dispersion regime

Optimal fibers	Pump wavelength (μm)	<i>D</i> (ps nm <sup>-1</sup> km <sup>-1</sup> )	<i>A<sub>eff</sub></i> (μm <sup>2</sup> )	<i>γ</i> (W <sup>-1</sup> km <sup>-1</sup> )	Attenuation (dB/cm)
Lanh et al. (2019)	1.03	-24	1.50	1290	0
Van et al. (2017)	1.55	-9.46	7.80	1200	1.92
Van et al. (2020)	1.56	-2.20	4.73	2000	2.40
Lanh et al. (2022)	1550	-3	2.04	1742	4.42
#CBF <sub>1</sub>	1.064	-17	1.33	7447	0.18
#SBF <sub>2</sub>	1.3	-19.90	1.84	5391	0.38
#HBF <sub>3</sub>	1.3	-0.89	1.88	5255	0.41

$$\partial_z \tilde{A} - i\tilde{\beta}(\omega)\tilde{A} - \frac{\tilde{\alpha}(\omega)}{2}\tilde{A} = i\gamma \left( 1 + \frac{\omega - \omega_0}{\omega_0} \right) \tilde{A} F \left[ \int_{-\infty}^{\infty} R(T') |A|^2 (T - T') dT' \right], \quad (4)$$

where  $\tilde{A}(\omega)$  describes the Fourier transform (FT) of an envelope pulse  $A(t)$ . The laser pulses used in the simulations are modeled by a Gaussian pulse centered at the pumping wavelength and are expressed as given in Eq. (5):

$$A(t) = \sqrt{P_0} \exp\left(-\frac{t^2}{2t_0^2}\right). \quad (5)$$

The effects of the linear propagation (the left side of Eq. 4) are determined by the reduction and *D* of the fiber. In our numerical modeling, the high-order dispersions are calculated through the Taylor series expansion coefficients of the propagation constant at the pumping pulse frequency:

$$\tilde{\beta}(\omega) = \beta(\omega) - \beta_0(\omega) - \omega \left. \frac{\partial \beta}{\partial \omega} \right|_{\omega=\omega_0} \tag{6}$$

The high order of dispersion is shown in Table 2. The right side of Eq. 4 models the effects of the nonlinearity. These effects are dependent upon the nonlinear optical response of benzene determined by the combination of bound-electronic and nuclear contributions. The Raman response function is given by Agrawal (2012), where  $f_R$  is a fraction of the delayed contribution,  $\delta(t)$  is the Dirac delta function, and  $R'(t)$  denotes the delayed nonlinear response:

$$R(t) = (1 - f_R)\delta(t) + f_R R'(t). \tag{7}$$

For the proposed fibers, pulses with a center wavelength ( $\lambda_p$ ) of 1.064  $\mu\text{m}$  (#CBF<sub>1</sub>), 1.3  $\mu\text{m}$  (#SBF<sub>2</sub>, #HBF<sub>3</sub>) with a duration ( $\tau$ ) of 40 fs are emitted by, for example, Menlo Systems C-fiber femtosecond erbium laser. The SCG is reproduced for 1 cm with different input peak power (P) in the range of 0.075–0.45 kW. The spectral intensity of the SCG is illustrated in Fig. 11.

Since #CBF<sub>1</sub>, #SBF<sub>2</sub>, and #HBF<sub>3</sub> operate in the regime of the all-normal dispersion, the self-phase modulation (SPM) followed by optical wave breaking (OWB) are the key phenomena, which contribute to generating SC (Dudley et al. 2006; Hooper et al. 2011; Takushima and Kikuchi 1999). When the input peak power is lower than 0.15 kW, the spectral expansion is due to the key contribution of the SPM. The symmetrical form of the incident pulse and the progression of an oscillating structure in the spectrum are the most notable features. The outermost peaks of the multi-peak spectrum are the strongest. In this case, because there is only the process of the SPM, the achieved spectrum expansion is very limited (Dudley and Taylor 2010; Heidt et al. 2017).

When the input peak power is higher than 0.15 kW, the OWB starts to appear. The contribution of OWB makes the spectral broadening process increase rapidly (Hoang et al. 2018; Van et al. 2020). With the same input peak power, #CBF<sub>1</sub> and #SBF<sub>2</sub> have a flatter spectral intensity than #HBF<sub>3</sub> but #HBF<sub>3</sub> has the largest spectral broadening range. Table 3 reports the comparison of SCG spectral broadening range of proposed fibers with those previously published. At extremely low input power of 0.45 kW, #CBF<sub>1</sub>, #SBF<sub>2</sub>, and #HBF<sub>3</sub> have SCG from 0.66–1.53, 0.71–1.76, and 0.71–1.82  $\mu\text{m}$ , respectively in visible light and near-infrared range. Meanwhile, other publications use input peak power that is 5–138 times larger than the one provided for our three

**Table 2** The coefficient of high order dispersion at the pump wavelength

Coefficients	#CBF <sub>1</sub>	#SBF <sub>2</sub>	#HBF <sub>3</sub>
$\beta_2$ (ps <sup>2</sup> /m)	$1.12 \times 10^{-2}$	$1.75 \times 10^{-2}$	$7.51 \times 10^{-4}$
$\beta_3$ (ps <sup>3</sup> /m)	$-1.29 \times 10^{-5}$	$-1.41 \times 10^{-4}$	$-1.36 \times 10^{-5}$
$\beta_4$ (ps <sup>4</sup> /m)	$5.10 \times 10^{-7}$	$1.00 \times 10^{-6}$	$2.99 \times 10^{-7}$
$\beta_5$ (ps <sup>5</sup> /m)	$-2.48 \times 10^{-9}$	$-3.86 \times 10^{-9}$	$8.82 \times 10^{-11}$
$\beta_6$ (ps <sup>6</sup> /m)	$1.99 \times 10^{-11}$	$2.18 \times 10^{-11}$	$1.21 \times 10^{-11}$
$\beta_7$ (ps <sup>7</sup> /m)	$7.09 \times 10^{-14}$	$8.07 \times 10^{-14}$	$-2.72 \times 10^{-13}$
$\beta_8$ (ps <sup>8</sup> /m)	$-3.65 \times 10^{-15}$	$-7.20 \times 10^{-15}$	$-3.94 \times 10^{-15}$
$\beta_9$ (ps <sup>9</sup> /m)	$-2.79 \times 10^{-17}$	$2.40 \times 10^{-17}$	$1.25 \times 10^{-16}$
$\beta_{10}$ (ps <sup>10</sup> /m)	$1.01 \times 10^{-18}$	$2.53 \times 10^{-18}$	$4.54 \times 10^{-19}$
$\beta_{11}$ (ps <sup>11</sup> /m)	$7.54 \times 10^{-21}$	$-3.09 \times 10^{-20}$	$-4.35 \times 10^{-20}$

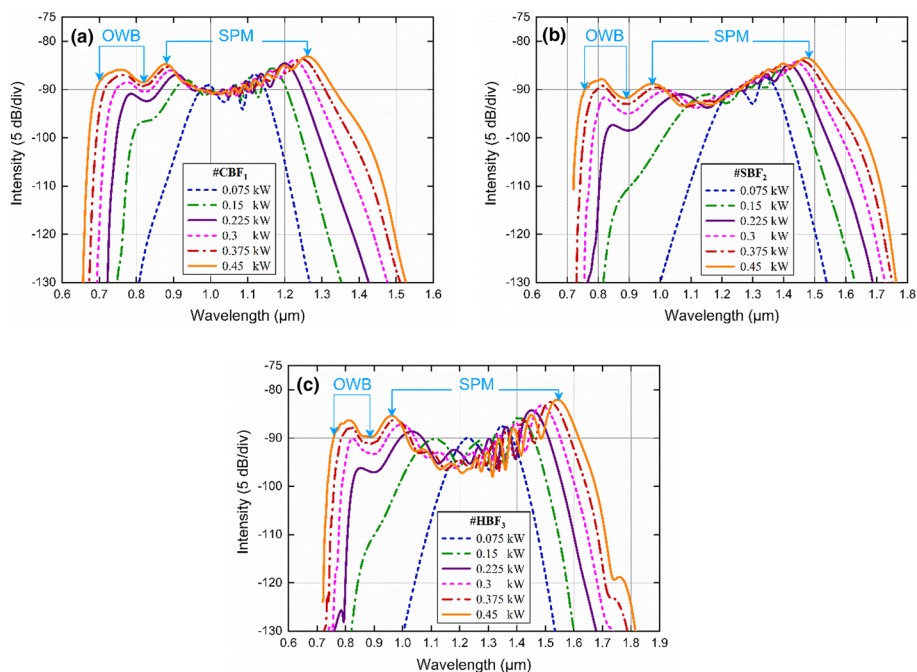


**Fig. 11** The spectral intensity of SCG with 40 fs duration, 1 cm fiber length, and different peak power in the range of 0.075–0.45 kW: **a** #CBF<sub>1</sub>; the pulse has central wavelength 1.064 μm, **b** #SBF<sub>2</sub>, and **c** #HBF<sub>3</sub> the pulses have a central wavelength of 1.3 μm

**Table 3** The SCG spectral broadening range compared with those previously published in the all-normal dispersion regime

Ref.	Liquid	$\lambda_p$ (μm)	$P$ (kW)	Fiber length (cm)	SCG range (μm)
This work	#CBF <sub>1</sub>	1.064	0.45	1	0.66–1.53
This work	#SBF <sub>2</sub>	1.3	0.45	1	0.71–1.76
This work	#HBF <sub>3</sub>	1.3	0.45	1	0.71–1.82
Fanjoux et al. (2017)	C <sub>7</sub> H <sub>8</sub>	0.532	11.11	60	0.55–0.87
Churin et al. (2013)	CS <sub>2</sub>	1.91	14.17	16	1.79–2.4
Hoang et al. (2018)	C <sub>7</sub> H <sub>8</sub>	1.03	25.00	10	0.95–1.1
Dinh et al. (2018)	CCl <sub>4</sub>	1.064	2.67	30	0.95–1.15
Hoang et al. (2019)	CCl <sub>4</sub>	1.03	62.50	20	0.85–1.25
Lanh et al. (2019)	CHCl <sub>3</sub>	1.03	2.50	20	0.6–1.26
Van et al. (2017)	C <sub>7</sub> H <sub>8</sub>	1.55	7.14	5	1.1–1.75
Lanh et al. (2022)	C <sub>6</sub> H <sub>5</sub> NO <sub>2</sub>	1.15	0.11	5	0.72–1.7
Lanh et al. (2022)	C <sub>6</sub> H <sub>5</sub> NO <sub>2</sub>	1.23	0.11	5	0.74–1.77
Lanh et al. (2022)	C <sub>6</sub> H <sub>5</sub> NO <sub>2</sub>	1.55	0.11	5	0.83–2.36

**Fig. 12** Spectral bandwidth versus different peak power

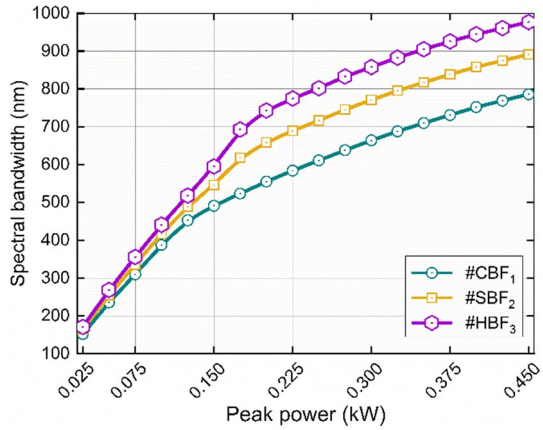


**Table 4** The spectral widths corresponding with peak power

<i>P</i> (kW)	#CBF <sub>1</sub>	#SBF <sub>2</sub>	#HBF <sub>3</sub>
0.075	310	336	356
0.15	491	546	595
0.225	584	695	775
0.3	664	776	858
0.375	731	844	926
0.45	786	897	977

fibers (Lanh et al. 2019; Hoang et al. 2019) but the spectrum only extends from 0.15 to 0.66 μm (Hoang et al. 2018; Lanh et al. 2019). With the use of low peak power ( $P=0.11$  kW), the SCG spectral bandwidth for the fibers in the publication (Lanh et al. 2022) is not too much larger than in this work (except for square lattice PCF). This is because the nonlinear refractive index of nitrobenzene is larger than that of benzene. However, we choose benzene as the liquid to infiltrate the core of PCFs due to its prevalence and less toxicity. In addition, the fiber sample length used herein is only 1 cm, which is 5 times shorter than those in Lanh et al. (2022), thus the cost can be reduced and the propagation loss can be considered negligible (Van et al. 2017).

Figure 12 presents the spectral broadening according to different values of the input peak power. We can see that, as the input peak power increases (or decreases), spectral broadening also increases (or decreases). In Table 4, we calculated the corresponding spectral widths for different input peak power values. At 0.45 kW peak power, #CBF<sub>1</sub>, #SBF<sub>2</sub>, and #HBF<sub>3</sub> have spectral widths of 0.786, 0.897, and 0.977 μm, respectively.

From the above results, it is shown that although #HBF<sub>3</sub> fiber has a larger effective mode area and attenuation than #CBF<sub>1</sub>, #SBF<sub>2</sub> fibers, its dispersion curve is flattest and is close to the zero-dispersion curve compared to the dispersion curves of #CBF<sub>1</sub>, #SBF<sub>2</sub> in the wavelength region 0.8–2.0 μm. These are the most important characteristics that determine the effectiveness of the SCG of #HBF<sub>3</sub>. Thus, optimizing the dispersion characteristic is the most important for SCG (Zhang et al. 2010; Van et al. 2017, 2020; Hoang et al. 2018; Hoang et al. 2019; Lanh et al. 2019; Dinh et al. 2018).

## 4 Conclusions

In the paper, the geometrical parameters of the BC-PCFs are optimized to obtain three structures with all-normal dispersive characteristics. The suggestive BC-PCFs have a coefficient of the high effective nonlinearity of  $7447 \text{ W}^{-1} \text{ km}^{-1}$  at  $1.064 \mu\text{m}$ ,  $5391 \text{ W}^{-1} \text{ km}^{-1}$ , and  $5255 \text{ W}^{-1} \text{ km}^{-1}$  at  $1.3 \mu\text{m}$ , for #CBF<sub>1</sub>, #SBF<sub>2</sub>, and #HBF<sub>3</sub>, respectively. The structured parameters of BC-PCFs have demonstrated the efficiency of high coupling between the fibers of the standard femtosecond and the highly nonlinear fiber. In our work, the SCG obtained high coherence with shorter fiber segments, only 1 cm, with a peak power of 0.45 kW and 40 fs pulse duration. The spectrum widths of #CBF<sub>1</sub>, #SBF<sub>2</sub>, and #HBF<sub>3</sub> are in the range of 0.66–1.53, 0.71–1.76, and 0.71–1.82  $\mu\text{m}$ , respectively. The SCG in all proposed PCFs is very suitable for standard femtosecond fiber lasers.

The structure is optimized to be compatible with a source of a priorate femtosecond laser, i.e., the low strict and attenuation dispersion for the wavelength of the centered pump. The #CBF<sub>1</sub> is optimized for sources operating at  $1.064 \mu\text{m}$ , while the #SBF<sub>2</sub> and #HBF<sub>3</sub> operate at the  $1.3 \mu\text{m}$  wavelength of the pumped sources. The non-linear processes occurring in the SCG in conventional systems are the same as those in several previous (Van et al. 2017, 2020; Hoang et al. 2018; Tan 1998; Lanh et al. 2022; Agrawal 2012; Fanjoux et al. 2017; Churin et al. 2013; Dinh et al. 2018). In our research, PCFs with HL have been proven to be the most effective for SCG applications. All of the studied fibers are good candidates for alternative all-fiber supercontinuum sources for glass-core fibers. It should be noted that all-fiber systems are strong, shock-proof, and neither includes an axis adjustable process nor an added pulse compressor.

**Acknowledgments** This research is funded by Vietnam's Ministry of Education and Training (B2021-DHH-08).

**Funding** The authors have not disclosed any funding.

**Data availability** No data availability statement.

## Declarations

**Conflict of interest** The authors declare that they have no conflict of interest.

## References

- Agrawal, G.: Nonlinear fiber optics. Academic Press (2012)
- Buczyński, R.: Photonic crystal fibers. *Acta Phys. Pol. A* **106**, 141–168 (2004)
- Churin, D., Nguyen, T.N., Kieu, K., Norwood, R.A., Peyghambarian, N.: Mid-IR supercontinuum generation in an integrated liquid core optical fiber filled with CS<sub>2</sub>. *Opt. Mater. Express* **3**, 1358–1364 (2013)
- Corwin, K.L., Newbury, N.R., Dudley, J.M., Coen, S., Diddams, S.A., Weber, K., Windeler, R.S.: Fundamental noise limitations to supercontinuum generation in microstructure fiber. *Phys. Rev. Lett.* **90**, 113904(1–4) (2003)
- Dinh, Q.H., Pniewski, J., Van, H.L., Ramaniuk, A., Long, V.C., Borzycki, K., Xuan, K.D., Klimczak, M., Buczynski, R.: Optimization of optical properties of photonic crystal fibers infiltrated with, carbon tetrachloride for supercontinuum generation with subnanjoule femtosecond pulses. *Appl. Opt.* **57**, 3738–3746 (2018)



- Dudley, J.M., Genty, G., Coen, S.: Supercontinuum generation in photonic crystal fiber. *J. Rev. Mod. Phys.* **78**, 1135–1184 (2006)
- Dudley, J.M., Taylor, J.R.: Supercontinuum generation in optical fibers. Cambridge University Press (2010)
- Fanjoux, G., Margueron, S., Beugnot, J.C., Sylvestre, T.: Supercontinuum generation by stimulated Raman-Kerr scattering in a liquid core optical fiber. *J. Opt. Soc. Am. B* **34**, 1677–1683 (2017)
- Hartl, I., Li, X.D., Chudoba, C., Ghanta, R.K., Ko, T.H., Fujimoto, J.G., Ranka, J.K., Windeler, R.S.: Ultrahigh-resolution optical coherence tomography using continuum generation in an air-silica microstructure optical fiber. *Opt. Lett.* **26**, 608–610 (2001)
- Heidt, A.M., Rothhardt, J., Hartung, A., Bartelt, H., Rohwer, E.G., Limpert, J., Tunnermann, A.: High quality sub-two cycle pulses from compression of supercontinuum generated in all-normal dispersion photonic crystal fiber. *Opt. Express* **19**, 13873–13879 (2011)
- Heidt, A.M., Feehan, J.S., Price, J.H.V., Feurer, T.: Limits of coherent supercontinuum generation in normal dispersion fibers. *J. Opt. Soc. Am. B* **34**, 764–775 (2017)
- Hoang, V.T., Kasztelanica, R., Anuszkiewicz, A., Stepniowski, G., Filipkowski, A., Ertman, S., Pysz, D., Wolinski, T., Xuan, K.D., Klimczak, M., Buczynski, R.: All-normal dispersion supercontinuum generation in photonic crystal fibers with large hollow cores infiltrated with toluene. *Opt. Mater. Express* **8**, 3568–3582 (2018)
- Hoang, V.T., et al.: Supercontinuum generation in an allnormal dispersion large core photonic crystal fiber infiltrated with carbon tetrachloride. *Opt. Mater. Express* **9**, 2264–2278 (2019)
- Hooper, L.E., Mosley, P.J., Muir, A.C., Wadsworth, W.J., Knight, J.C.: Coherent supercontinuum generation in photonic crystal fiber with all-normal group velocity dispersion. *Opt. Express* **19**, 4902–4907 (2011)
- <https://www.lumerical.com/products/mode/>
- Isobe, K., Suda, A., Tanaka, M., Hashimoto, H., Kannari, F., Kawano, H., Mizuno, H., Miyawaki, A., Midorikawa, K.: Single-pulse coherent anti-Stokes Raman scattering microscopy employing an octave spanning pulse. *Opt. Express* **17**, 1259–11266 (2009)
- Kano, H., Hamaguchi, H.: Ultrabroadband ( $> 2500 \text{ cm}^{-1}$ ) multiplex coherent anti-Stokes Raman scattering microspectroscopy using a supercontinuum generated from a photonic crystal fiber. *Appl. Phys. Lett.* **86**, 121113(1–3) (2005)
- Knight, J.C., Birks, T.A., Russell, P.S.J., Atkin, D.M.: All-silica single-mode optical fiber with photonic crystal cladding. *Opt. Lett.* **21**, 1547–1549 (1996)
- Lanh, C.V., Hoang, V.T., Long, V.C., Borzycki, K., Xuan, K.D., Quoc, V.T., Trippenbach, M., Buczyński, R., Pniowski, J.: Optimization of optical properties of photonic crystal fibers infiltrated with chloroform for supercontinuum generation. *Laser Phys.* **29**, 075107(1–9) (2019)
- Lanh, C.V., Thuy, N.T., Duc, H.T., Tran, L.T.B., Ngoc, V.T.M., Trong, D.V., Trung, L.C., Quang, H.D., Khoa, D.Q.: Comparison of supercontinuum spectrum generating by hollow core PCFs filled with nitrobenzene with different lattice types. *Opt. Quant. Electro.* **54**, 300(1–17) (2022)
- Medjouri, A., Simohamed, L.M., Ziane, O., Boudrioua, A.: Analysis of a new circular photonic crystal fiber with large mode area. *Optik* **126**, 5718–5724 (2015)
- Mogilevtsev, D., Birks, T.A., Russell, P.S.J.: Group-velocity dispersion in photonic crystal fibers. *Opt. Lett.* **23**, 1662–1664 (1998)
- Monfared, Y.E., Javan, A.R.M., Kashani, A.R.M.: Confinement loss in hexagonal lattice photonic crystal fibers. *Optik* **124**, 7049–7052 (2013)
- Moutzouris, K., Papamichael, M., Betsis, S.C., Stavarakas, I., Hloupis, G., Triantis, D.: Refractive, dispersive and thermo-optic properties of twelve organic solvents in the visible and near-infrared. *Appl. Phys. B* **116**, 617–622 (2014)
- Myers, T.L., Tonkyn, R.G., Danby, T.O., Taubman, M.S., Bernacki, B.E., Birnbaum, J.C., Sharpe, S.W., Johnson, T.J.: Accurate measurement of the optical constants  $n$  and  $k$  for a series of 57 inorganic and organic liquids for optical modeling and detection. *Appl. Spectrosc.* **72**, 535–550 (2018)
- Nibbering, E.T.J., Franco, M.A., Prade, B.S., Grillon, G., Blanc, C.L., Mysyrowicz, A.: Measurement of the nonlinear refractive index of transparent materials by spectral analysis after nonlinear propagation. *Opt. Commun.* **119**, 479–484 (1995)
- Pandey, S.K., Prajapati, Y.K., Maur, J.B.: Design of simple circular photonic crystal fiber having high negative dispersion and ultra-low confinement loss. *Results Opt.* **1**, (100024) 1–7 (2020)
- Pysz, D., Kujawa, I., Stepien, R., Klimczak, M., Filipkowski, A., Franczyk, M., Kociszewski, L., Buzniak, J., Harasny, K., Buczynski, R.: Stack and draw fabrication of soft glass microstructured fiber optics. *Bull. Pol. Acad. Sci. Tech. Sci.* **62**, 667–682 (2014)
- Qian, K., Gu, Z., Xu, J., Dong, X., Yu, W., Yu, Z., Ren, D.: Noise-like pulse erbium-doped fiber laser for supercontinuum generation. *Optik* **158**, 215–219 (2018)

- Ranka, J.K., Windeler, R.S., Stentz, A.J.: Visible continuum generation in air silica microstructure optical fibers with anomalous dispersion at 800 nm. *Opt. Lett.* **25**, 25–27 (2000)
- Saghaei, H.: Supercontinuum source for dense wavelength division multiplexing in square photonic crystal fiber via fluidic infiltration approach. *Radioengineering* **26**, 16–22 (2017)
- Saitoh, K., Koshiba, M., Hasegawa, T., Sasaoka, E.: Chromatic dispersion control in photonic crystal fibers: application to ultra-flattened dispersion. *Opt. Express* **11**, 843–852 (2003)
- Sen, S., Shafi, M.A., Kabir, M.A.: Hexagonal photonic crystal fiber (H-PCF) based optical sensor with high relative sensitivity and low confinement loss for terahertz (THz) regime. *Sensing and Bio-Sensing Research* **30**, (100377) 1–9 (2020)
- Takushima, Y., Kikuchi, K.: 10-GHz, over 20-channel multiwavelength pulse source by slicing super-continuum spectrum generated in normal-dispersion fiber. *IEEE Photonics Technol. Lett.* **11**, 322–324 (1999)
- Tan, C.Z.: Determination of refractive index of silica glass for infrared wavelengths by IR spectroscopy. *J. Non-Cryst. Solids* **223**, 158–163 (1998)
- Tran, L.T.B., Thuy, N.T., Ngoc, V.T.M., Trung, L.C., Minh, L.V., Van, C.L., Khoa, D.X., Lanh, C.V.: Analysis of dispersion characteristics of solid-core PCFs with different types of lattices in the claddings, infiltrated with ethanol. *Photonics Lett. Pol.* **12**, 106–108 (2020)
- Tu, H., Liu, Y., Turchinovich, D., Boppart, S.A.: Compression of fiber supercontinuum pulses to the Fourier-limit in a high-numerical-aperture focus. *Opt. Lett.* **36**, 2315–2317 (2011)
- Udem, T., Holzwarth, R., Hansch, T.W.: Optical frequency metrology. *Nature* **416**, 233–237 (2002)
- Ulman, M., Bailey, D.W., Acioli, L.H., Vallee, F.G., Stanton, C.J., Ippen, E.P., Fujimoto, J.G.: Femtosecond tunable nonlinear absorption spectroscopy in  $\text{Al}_{0.1}\text{Ga}_{0.9}\text{As}$ . *Phys. Rev. B* **47**, 10267–10278 (1993)
- Van, L.C., Anuszkiewicz, A., Ramaniuk, A., Kasztelanica, R., Dinh, K.X., Trippenbach, M., Buczynski, R.: Supercontinuum generation in photonic crystal fibres with core filled with toluene. *J. Opt.* **19**, (125604) 1–9 (2017)
- Van, L.C., Hoang, V.T., Borzycki, K., Xuan, K.D., Quoc, V.T., Trippenbach, M., Buczyński, R., Pniewski, J.: Supercontinuum generation in photonic crystal fibers infiltrated with nitrobenzene. *Laser Phys.* **30**, (035105) 1–9 (2020)
- Vieweg, M., Gissibl, T., Pricking, S., Kuhlmeier, B.T., Wu, D.C., Eggleton, B.J., Giessen, H.: Ultrafast nonlinear optofluidics in selectively liquid-filled photonic crystal fibers. *Opt. Express* **18**, 25232–25240 (2010)
- Zhang, H., Chang, S., Yuan, J., Huang, D.: Supercontinuum generation in chloroform-filled photonic crystal fibers. *Optik* **121**, 783–787 (2010)

**Publisher's Note** Springer Nature remains neutral with regard to jurisdictional claims in published maps and institutional affiliations.

Springer Nature or its licensor holds exclusive rights to this article under a publishing agreement with the author(s) or other rightsholder(s); author self-archiving of the accepted manuscript version of this article is solely governed by the terms of such publishing agreement and applicable law.